

Nonhelical inverse transfer of a decaying turbulent magnetic field

Axel Brandenburg,^{1,2,*} Tina Kahniashvili,^{3,4,5,†} and Alexander G. Tevzadze^{6,‡}

¹*Nordita, KTH Royal Institute of Technology and Stockholm University, Roslagstullsbacken 23, 10691 Stockholm, Sweden*

²*Department of Astronomy, AlbaNova University Center, Stockholm University, 10691 Stockholm, Sweden*

³*The McWilliams Center for Cosmology and Department of Physics,*

Carnegie Mellon University, 5000 Forbes Ave, Pittsburgh, PA 15213, USA

⁴*Department of Physics, Laurentian University, Ramsey Lake Road, Sudbury, ON P3E 2C, Canada*

⁵*Abastumani Astrophysical Observatory, Ilia State University,*

3-5 Cholokashvili Ave, Tbilisi, GE-0194, Georgia

⁶*Faculty of Exact and Natural Sciences, Tbilisi State University, 1 Chavchavadze Ave., Tbilisi, 0128, Georgia*

(Dated: September 12, 2018, Revision: 1.4)

In the presence of magnetic helicity, inverse transfer from small to large scales is well known in magnetohydrodynamic (MHD) turbulence and has applications in astrophysics, cosmology, and fusion plasmas. Using high resolution direct numerical simulations of magnetically dominated self-similarly decaying MHD turbulence, we report a similar inverse transfer even in the absence of magnetic helicity. We compute for the first time spectral energy transfer rates to show that this inverse transfer is about half as strong as with helicity, but in both cases the magnetic gain at large scales results from velocity at similar scales interacting with smaller-scale magnetic fields. This suggests that both inverse transfers are a consequence of a universal mechanisms for magnetically dominated turbulence. Possible explanations include inverse cascading of the mean squared vector potential associated with local near two-dimensionality and the shallower k^2 subinertial range spectrum of kinetic energy forcing the magnetic field with a k^4 subinertial range to attain larger-scale coherence. The inertial range shows a clear k^{-2} spectrum and is the first example of fully isotropic magnetically dominated MHD turbulence exhibiting weak turbulence scaling.

PACS numbers: 98.70.Vc, 98.80.-k

The nature of magnetohydrodynamic (MHD) turbulence has received significant attention in recent years [1]. Whenever plasma is ionized, it is electrically conducting and Kolmogorov's turbulence theory [2] has to be replaced by an appropriate theory for MHD turbulence [3]. This becomes relevant under virtually all astrophysical circumstances. However, the universal character of MHD turbulence is debated and several fundamental questions remain unanswered: how do kinetic and magnetic energy spectra look like and are they similar? How does this depend on the magnetic Prandtl number, $\text{Pr}_M = \nu/\eta$, i.e., the ratio of kinematic viscosity and magnetic diffusivity? What is the role of the Alfvén effect, i.e., how does the presence of a finite Alfvén speed v_A enter the expression for the turbulent energy spectrum?

If the spectral properties of MHD turbulence are governed solely by the rate of energy transfer ϵ , we know from dimensional arguments that the spectrum must scale as $E(k) \sim \epsilon^{2/3} k^{-5/3}$ with wavenumber k . However, MHD turbulence becomes increasingly anisotropic toward small scales [4], so the spectrum $E(k_\perp, k_\parallel)$ depends on the wavenumbers perpendicular and parallel to the magnetic field \mathbf{B} , and is essentially given by $\epsilon^{2/3} k_\perp^{-5/3}$, so most of the energy cascades perpendicular to \mathbf{B} .

In the case of forced turbulence, direct numerical simulations (DNS) show similar spectra both with imposed [1] and dynamo-generated [5] fields. However, when \mathbf{B} is decaying, the result depends on the value of the initial ratio v_A/u_{rms} of root mean square (rms) Alfvén speed to rms turbulent velocity. Recent DNS [6] found numerical evidence for three different scalings: Iroshnikov–Kraichnan scaling [7] proportional to $(\epsilon v_A)^{1/2} k^{-3/2}$ for $v_A/u_{\text{rms}} = 0.9$, Goldreich–Sridhar scaling [4] proportional to $\epsilon^{2/3} k_\perp^{-5/3}$ for $v_A/u_{\text{rms}} = 1.3$, and weak turbulence scaling [8] proportional to $(\epsilon v_A k_\parallel)^{1/2} k_\perp^{-2}$ for $v_A/u_{\text{rms}} = 2.0$; see Ref. [9] for a comparison of these three scalings. However, their physical interpretation is subject to criticism in that dynamic alignment between \mathbf{u} and \mathbf{B} can be responsible for the shallower $k^{-3/2}$ scaling [10] and the k^{-2} scaling could also be caused by a dominance of discontinuities [11].

It is usually taken for granted that for non-helical turbulence, energy is cascading toward small scales. An inverse cascade has so far only been found for helical turbulence [3, 12] and was confirmed in DNS [13–15]. It is evident that this requires significant scale separation, $k_0/k_1 \gg 1$, where k_0 is the wavenumber of the peak of the spectrum and $k_1 = 2\pi/L$ is the minimal wavenumber of the domain of size L . Since an inverse transfer was not expected to occur in the absence of helicity, most previous work did not allow for $k_0/k_1 \gg 1$. However, when k_0/k_1 is moderate, some inverse cascading was found [14]. The present work shows that this behavior is genuine and

*Electronic address: brandenb@nordita.org

†Electronic address: tinatin@phys.ksu.edu

‡Electronic address: aleko@tevza.org

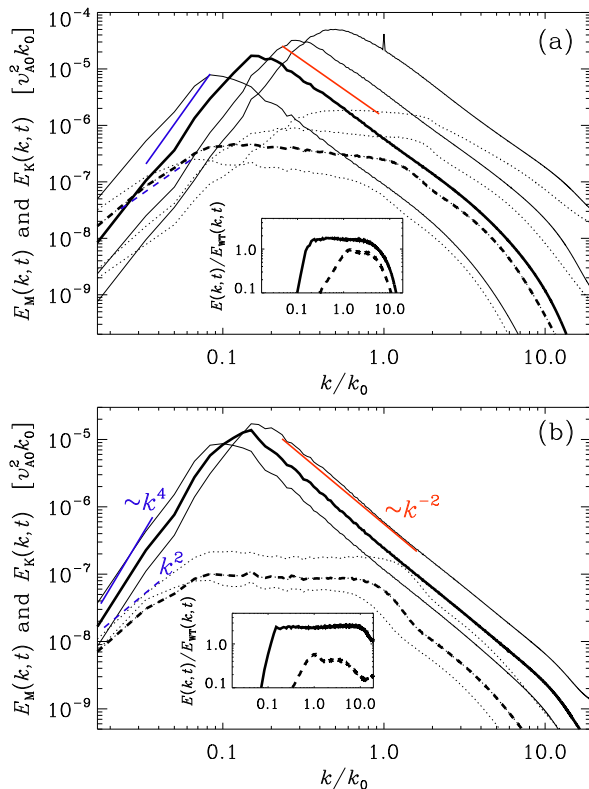


FIG. 1: (Color online) (a) Magnetic (solid lines) and kinetic (dashed lines) energy spectra for Run A at times $t/\tau_A = 18, 130, 450,$ and 1800 ; the time $t/\tau_A = 450$ is shown as bold lines. The straight lines indicate the slopes k^4 (solid, blue), k^2 (dashed, blue), and k^{-2} (red, solid). (b) Same for Run B, at $t/\tau_A = 540, 1300,$ and 1800 , with $t/\tau_A = 1300$ shown as bold lines. The insets show E_M and E_K compensated by E_{WT} .

more pronounced at higher resolution, larger Reynolds numbers and larger k_0/k_1 .

We solve the compressible MHD equations for \mathbf{u} , the gas density ρ at constant sound speed c_s , and the magnetic vector potential \mathbf{A} , so $\mathbf{B} = \nabla \times \mathbf{A}$. Following our earlier work [16–18], we initialize our decaying DNS by restarting them from a snapshot of a driven DNS, where a random forcing was applied in the evolution equation for \mathbf{A} rather than \mathbf{u} . To allow for sufficient scale separation, we take $k_0/k_1 = 60$. We use the PENCIL CODE [19] at a resolution of 2304^3 meshpoints on 9216 processors. The code uses sixth order finite differences and a third order accurate time stepping scheme.

Our magnetic and kinetic energy spectra are normalized such that $\int E_M(k, t) dk = \mathcal{E}_M(t) = v_A^2/2$ and $\int E_K(k, t) dk = \mathcal{E}_K(t) = v_{\text{rms}}^2/2$ are magnetic and kinetic energies per unit mass. The magnetic integral scale is defined as $\xi_M = k_M^{-1}(t) = \int k^{-1} E_M(k, t) dk / \mathcal{E}_M(t)$. Time is given in initial Alfvén times $\tau_A = (v_{A0} k_0)^{-1}$, where $v_{A0} = v_A(0)$. In Fig. 1 we show $E_M(k, t)$ and $E_K(k, t)$ for Runs A and B (restarted from A at $t/\tau_A = 450$) with $\text{Pr}_M = 1$ and 10 , respectively, and in Fig. 2 slices $B_z(x, y)$

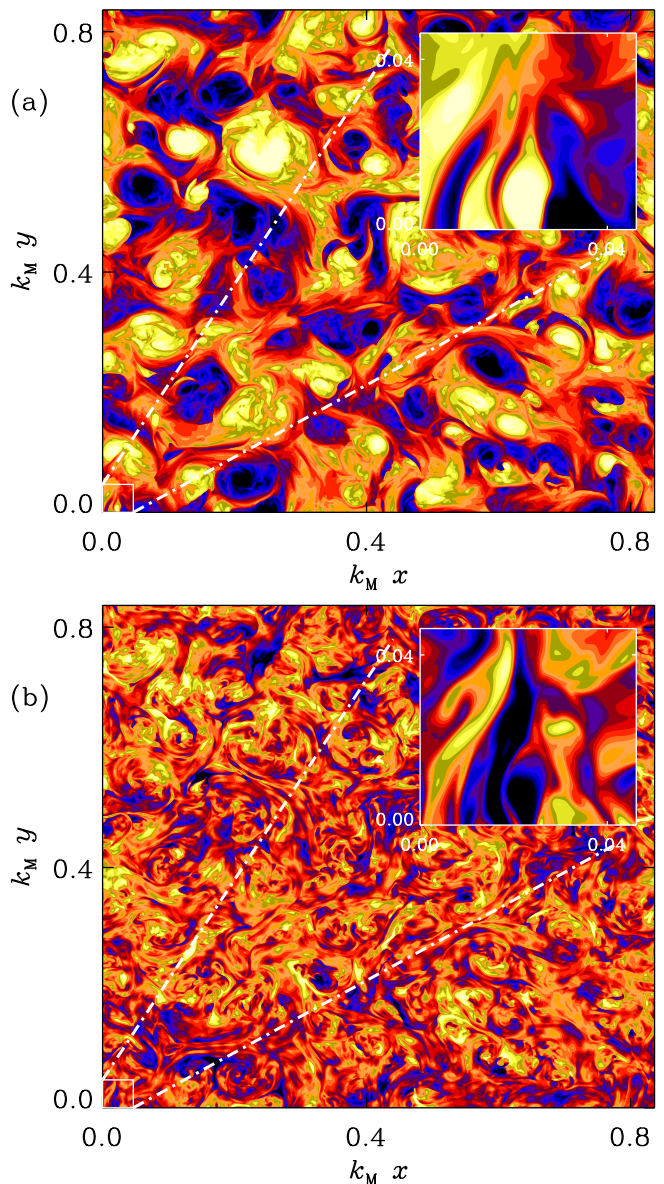


FIG. 2: (Color online) Contours of (a) $B_z(x, y)$ and (b) $u_z(x, y)$ for Run A. The insets show a zoom into the small square in the lower left corner.

and $u_z(x, y)$ at $z = 0$ at the last time Run A. We find an inertial range with weak turbulence scaling,

$$E_{WT}(k, t) = C_{WT}(\epsilon v_A k_M)^{1/2} k^{-2}, \quad (1)$$

where $k_M^{-1}(t) = \int k^{-1} E_M(k, t) dk / \mathcal{E}_M(t)$ is the integral scale and k_M has been used in place of k_{\parallel} . The prefactor is $C_{WT} \approx 1.9$ for $\text{Pr}_M = 1$ and ≈ 2.4 for $\text{Pr}_M = 10$; see the insets. In agreement with earlier work [3, 17], \mathcal{E}_M decays like t^{-1} .

At small wavenumbers the k^4 and k^2 subinertial ranges respectively for $E_M(k, t)$ and $E_K(k, t)$ are carried over from the initial conditions. The k^4 Batchelor spectrum is in agreement with the causality requirement [20, 21]

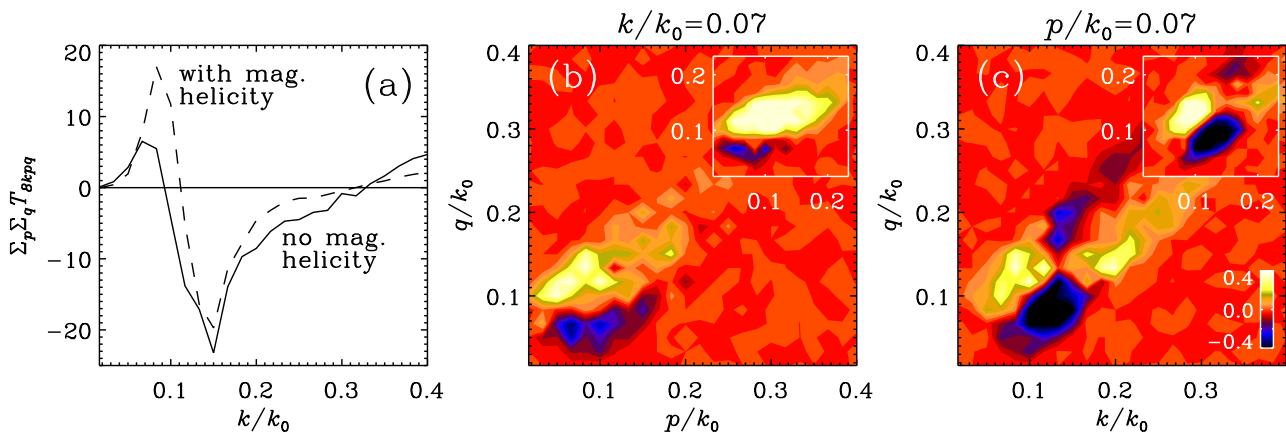


FIG. 3: (Color online) Spectral transfer function T_{kpq} , (a) as a function of k and summed over all p and q , (b) as a function of p and q for $k/k_1 = 4$, and (c) as a function of k and q for $p/k_1 = 4$. The dashed line in (a) and the insets in (b) and (c) show the corresponding case for a DNS with helicity; both for $\text{Pr}_M = 1$.

for the divergence-free vector field \mathbf{B} . The velocity is driven entirely by the magnetic field and follows a white noise spectrum, $E_K(k) \propto k^2$ [21]. The resulting difference in the scaling implies that, although magnetic energy dominates over kinetic, the two spectra must cross at sufficiently small wavenumbers. This idea may also apply to incompressible [22] and relativistic [23] simulations, where inverse nonhelical transfer has recently been confirmed.

To quantify the nature of inverse transfer we show in Fig. 3 representations of the spectral transfer function $T_{kpq} = \langle \mathbf{J}^k \cdot (\mathbf{u}^p \times \mathbf{B}^q) \rangle$ and compare with the corresponding helical case of Ref. [18], but with 1024^3 mesh points and at a comparable time. Here, the superscripts indicate the radius of a shell in wavenumber space of Fourier filtered vector fields; see Ref. [15] for such an analysis in driven helical turbulence. The transfer function T_{kpq} quantifies the gain of magnetic energy at wavenumber k from interactions of velocities at wavenumber p and magnetic fields at wavenumber q . Fig. 3(a) shows a gain for $k/k_0 < 0.1$, which is about half of that for the helical case. The corresponding losses for $k/k_0 > 0.1$ are about equal in the two cases. In both cases, the magnetic gain at $k/k_0 = 0.07 = 4/60$ results from \mathbf{u}^p with $0 < p/k_0 < 0.2$ interacting with \mathbf{B}^q at $q/k_0 > 0.1$; see the light yellow shades in Fig. 3(b). Note that work done by the Lorentz force is $\langle \mathbf{u}^p \cdot (\mathbf{J}^k \times \mathbf{B}^q) \rangle = -T_{kpq}$. Thus, negative values of T_{kpq} quantify the gain of kinetic energy at wavenumber p from interactions of magnetic fields at wavenumbers k and q . Blue dark shades in Fig. 3(c) indicate therefore that the gain of kinetic energy at $p/k_0 = 0.07$ results from magnetic interactions at wavenumbers k and q of around $0.1 k_0$. These results support the interpretation that the increase of spectral power at large scales is similar to the inverse transfer in the helical case; see [24] for information concerning the total energy transfer.

To exclude that the inverse energy transfer is a con-

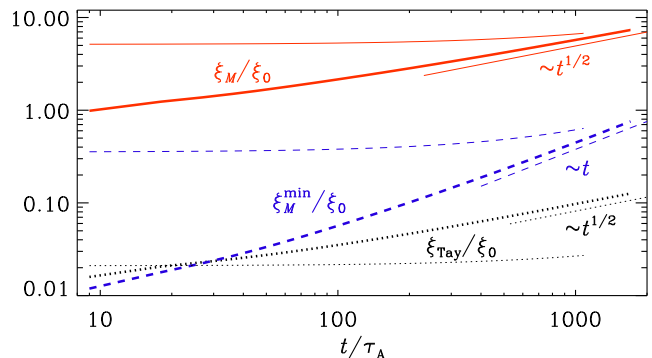


FIG. 4: Time evolution of $\xi_M = k_M^{-1}$ and ξ_M^{\min} , as well as the Taylor microscale ξ_{Tay} . Fat (thin) lines are for Run A (B).

sequence of the invariance of magnetic helicity, $\mathcal{H}_M(t) = \langle \mathbf{A} \cdot \mathbf{B} \rangle$, we compare ξ_M with its lower bound $\xi_M^{\min} = |\mathcal{H}_M|/2\mathcal{E}_M$ [17]; see Fig. 4. In nonhelical MHD turbulence, ξ_M is known to grow like $t^{1/2}$ [3, 17]. Even though the initial condition was produced with nonhelical plane waves, we find $\mathcal{H}_M \neq 0$ due to fluctuations. Since \mathcal{H}_M is conserved and \mathcal{E}_M decays like t^{-1} [3, 17], ξ_M^{\min} grows linearly and faster than $\xi_M \sim t^{1/2}$, so they will meet at $t/\tau_A = 10^5$ and then continue to grow as $t^{-2/3}$ [3, 17], but at $t/\tau_A = 10^3$ this cannot explain the inverse transfer. By contrast, we cannot exclude the possibility of the quasi two-dimensional mean squared vector potential, $\langle \mathbf{A}_{2D}^2 \rangle$, being approximately conserved [24]. This could explain the $\xi_M \sim t^{1/2}$ scaling and the inverse transfer if the flow was locally two-dimensional [25].

Since u_{rms} , v_A , and k_M are all proportional to $t^{-1/2}$ the decay is self-similar in such a way that the Reynolds and Lundquist numbers, $\text{Re} = u_{\text{rms}}/\nu k_M$ and $\text{Lu} = v_A/\eta k_M$, remain constant. Since $\mathcal{E}_K \ll \mathcal{E}_M$, the dissipated energy comes predominantly from $-d\mathcal{E}_M/dt$, and yet a substantial fraction of it is used to drive kinetic energy by per-

TABLE I: Comparison of relative dissipation rates, energies and other parameters for the two simulations discussed.

Run	Pr_M	v_{A0}/c_s	u_{rms}/v_A	Lu	Re	ϵ_K/ϵ_M	ϵ_M/ϵ	ϵ_K/ϵ
A	1	0.15	0.36	700	230	0.52	0.66	0.34
B	10	0.03	0.21	6300	130	0.93	0.52	0.48

forming work on the Lorentz force. Nevertheless, the viscous to magnetic dissipation ratio ϵ_K/ϵ_M increases only by a factor of 1.8 as Pr_M increases from 1 to 10; see Table I. This is less than for kinetically driven MHD turbulence, where $\epsilon_K/\epsilon_M \propto \text{Pr}_M^n$ with $n = 0.3\text{--}0.7$ [26]. Therefore, ϵ_M is here larger than in driven MHD turbulence, where large Lu can still be tolerated. This suggests that Run B may be under-resolved, which might also explain why it did not reach asymptotic scaling in Fig. 4.

In summary, we have shown that inverse transfer is a ubiquitous phenomenon of both helical and non-helical MHD. For helical MHD, this has been well known for nearly four decades [12], but for nonhelical MHD there have only been some low resolution DNS [14, 18]. Our DNS confirm an early finding by Olesen [27] that this inverse transfer occurs for all initial spectra that are sufficiently steep. His argument applies to hydrodynamic and MHD turbulence if the two spectra are parallel to each other. In our case, however, owing to the shallower k^2 spectrum of kinetic energy, kinetic energy always dominates over magnetic at large enough length scales. Either this or the near-conservation of $\langle A_{2D}^2 \rangle$ could be responsible for inverse transfer in magnetically dominated turbulence. This process is significant for cosmology and astrophysics [23], with applications not only to primordial magnetic fields, but also to ejecta from young stars, supernovae, and active galactic nuclei [28].

Our results support the idea of the weak turbulence k^{-2} scaling for strong magnetic field that is here for the first time globally isotropic and not an imposed one [29]. At small scales, however, approximate equipartition is still possible. The decay is slower than for usual MHD turbulence which is arguably governed by the Loitsyansky invariant [30]. Future investigations of the differences between these types of turbulence are warranted [24]. Interestingly, the extended plateau in the velocity spectrum around the position of the magnetic peak may be important for producing observationally detectable broad gravitational wave spectra [31].

We appreciate useful discussions with A. Neronov. Computing resources have been provided by the Swedish National Allocations Committee at the Center for Parallel Computers at the Royal Institute of Technology and by the Carnegie Mellon University Supercomputer Center. We acknowledge support from the Swedish Research Council grants 621-2011-5076 and 2012-5797, the European Research Council AstroDyn Project 227952, the Re-

search Council of Norway FRINATEK grant 231444, the Swiss NSF grant SCOPES IZ7370-152581, the NSF grant AST-1109180, and the NASA Astrophysics Theory Program grant NNX10AC85G. A.B. and A.T. acknowledge the hospitality of the McWilliams Center for Cosmology.

-
- [1] W. H. Matthaeus, S. Ghosh, S. Oughton, and D. A. Roberts, *J. Geophys. Res.* **101**, 7619 (1996); J. Cho and E.T. Vishniac, *Astrophys. J.* **538**, 217 (2000); J. Maron and P. Goldreich, *Astrophys. J.* **554**, 1175 (2001).
 - [2] A. Kolmogorov, *Dokl. Akad. Nauk SSSR*, **30**, 301 (1941);
 - [3] D. Biskamp and W.-C. Müller, *Phys. Rev. Lett.* **83**, 2195 (1999).
 - [4] P. Goldreich and S. Sridhar, *Astrophys. J.* **438**, 763 (1995).
 - [5] N. E. L. Haugen, A. Brandenburg, and W. Dobler, *Phys. Rev. E* **70**, 016308 (2004).
 - [6] E. Lee, M. E. Brachet, A. Pouquet, P. D. Mininni, D. Rosenberg, *Phys. Rev. E* **81**, 016318 (2010).
 - [7] R. S. Iroshnikov, *Sov. Astron.* **7**, 566 (1963); R. H. Kraichnan, *Phys. Fluids* **8**, 1385 (1965).
 - [8] S. Galtier, S.V. Nazarenko, A.C. Newell, and A. Pouquet, *J. Plasm. Phys.* **63**, 447 (2000).
 - [9] A. Brandenburg and Å. Nordlund, *Rep. Prog. Phys.* **74**, 046901 (2011); W. H. Matthaeus, D. C. Montgomery, M. Wan, and S. Servidio, *J. Turb.* **13**, N37 (2012).
 - [10] J. Mason, F. Cattaneo, and S. Boldyrev, *Phys. Rev. Lett.* **97**, 255002 (2006).
 - [11] V. Dallas and A. Alexakis, *Astrophys. J.* **788**, L36 (2014).
 - [12] A. Pouquet, U. Frisch, and J. Léorat, *J. Fluid Mech.* **77**, 321 (1976).
 - [13] D. Balsara and A. Pouquet, *Phys. Plasmas* **6**, 89 (1999).
 - [14] M. Christensson, M. Hindmarsh, and A. Brandenburg, *Phys. Rev. E* **70**, 056405 (2001).
 - [15] A. Brandenburg, *Astrophys. J.* **550**, 824 (2001).
 - [16] T. Kahniashvili, A. Brandenburg, A. G. Tevzadze and B. Ratra, *Phys. Rev. D* **81**, 123002 (2010).
 - [17] A. G. Tevzadze, L. Kisslinger, A. Brandenburg and T. Kahniashvili, *Astrophys. J.* **759**, 54 (2012).
 - [18] T. Kahniashvili, A. G. Tevzadze, A. Brandenburg and A. Neronov, *Phys. Rev. D* **87**, 083007 (2013); note that in their Eq. (14), \mathbf{v}/η should read $\partial\mathbf{v}/\partial\eta$.
 - [19] <http://pencil-code.googlecode.com/>
 - [20] R. Durrer and C. Caprini, *JCAP* **0311**, 010 (2003).
 - [21] P. A. Davidson, *Turbulence* (Oxford Univ. Press, 2004).
 - [22] A. Berera and M. Linkmann, *Phys. Rev. E* **90**, 041003 (2014).
 - [23] J. Zrake, *Astrophys. J.* **794**, L26 (2014).
 - [24] See Supplemental Material in arXiv:1404.2238 for details.
 - [25] A. Pouquet, *J. Fluid Mech.* **88**, 1 (1978).
 - [26] A. Brandenburg, *Astrophys. J.* **791**, 12 (2014).
 - [27] P. Olesen, *Phys. Lett. B* **398**, 321 (1997).
 - [28] A. M. Beck, K. Dolag, H. Lesch, and P. P. Kronberg, *Mon. Not. R. Astron. Soc.* **435**, 3575 (2013).
 - [29] J.C. Perez and S. Boldyrev, *Astrophys. J. Lett.* **672**, L61 (2008).
 - [30] P. A. Davidson, *J. Turb.* **1**, 006 (2000).
 - [31] T. Kahniashvili, L. Campanelli, G. Gogoberidze, Y. Maravin, and B. Ratra, *Phys. Rev. D* **78**, 123006 (2008).

Supplemental Material

The subject of magnetically dominated decaying MHD turbulence is relevant to the early Universe and has received enhanced attention in recent years. The focus of our Letter [1] is the investigation of inverse transfer of magnetic energy at the expense of kinetic energy at intermediate scales. In this Supplemental Material, we present additional details of the resulting turbulence regarding initial conditions, decay rate, the mechanisms for inverse transfer, including the question of local two-dimensionality of the turbulence, and the spectral energy transfer functions.

The simulations discussed in the Letter are motivated by applications to the early Universe such as the time of the electroweak phase transition. As shown in Ref. [2], the usual MHD equations can be applied when time t being replaced by the conformal time $\tilde{t} = \int dt/R(t)$, where $R(t)$ is the scale factor in the assumed flat, isotropic, homogeneous Universe as described by the Robertson-Walker metric.

Initial condition

Initial conditions can be obtained either as a result of an earlier turbulence simulation driven by monochromatic driving or the fields can be synthesized with given power spectra and random phases. In the following, we describe and compare these different cases.

Via monochromatic driving

Our goal is to have an initial condition that quickly leads to self-similar decay. Earlier experience [3–5] has shown that this is easily achieved by using a snapshot from a turbulence simulation that was driven with stochastic monochromatic forcing in the equation for the magnetic vector potential. The resulting initial condition used in our present work is shown in Fig. 5. It shows approximate k^2 and k^4 subinertial ranges for kinetic and magnetic energy spectra, respectively. Both spectra are maintained also at later times in such a way that they gradually shift upward with time (see Fig. 1 of the Letter).

In the present simulations (Run A of the Letter), both magnetic and kinetic energies show a slight uprise of power near the Nyquist wavenumber, $k_{\text{Ny}} = \pi/\delta x$, where δx is the mesh spacing. This indicates that the resolution is only marginal for the Reynolds number chosen here. However, during the subsequent decay calculation, after several Alfvén times, this excess power at k_{Ny} disappears, as is seen in Fig. 1 of the Letter.

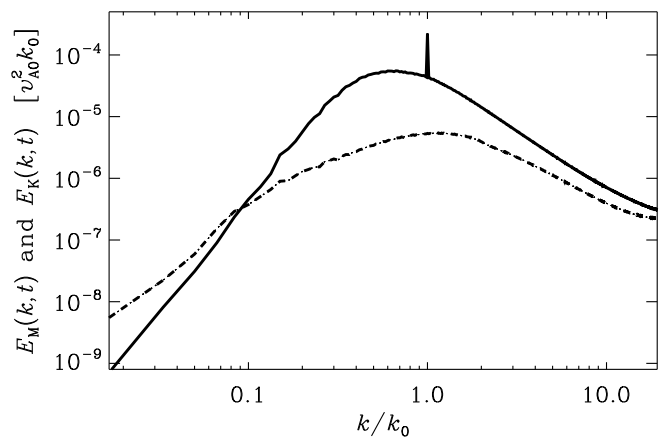


FIG. 5: Magnetic (solid lines) and kinetic (dashed lines) energy spectra for the initial condition of Run A.

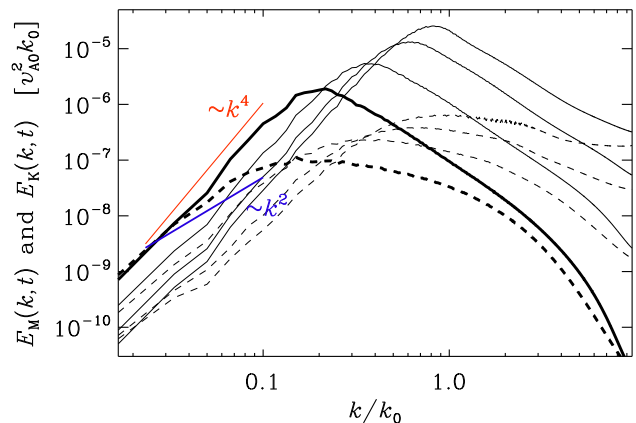


FIG. 6: Like Fig. 5, but with an initial k^4 spectrum for the magnetic energy using random phases.

Via random phases

An alternative mechanism of producing initial conditions is to generate a vector field in wavenumber space with a given spectrum and random phases. In Fig. 6 we show an example where we have for magnetic energy a k^4 spectrum for $k < k_0$ and $k^{-5/3}$ for $k > k_0$, but zero kinetic energy. Our initial velocity is zero and the initial vector potential in Fourier space is $\hat{A}_j(\mathbf{k})$ such that for all three components j are given by

$$k \hat{A}_j(\mathbf{k}) = A_0 \frac{(k/k_0)^{n_1/4-1/2}}{[1 + (k/k_0)^{n_1-n_2}]^{1/4}} e^{i\phi(\mathbf{k})}, \quad (2)$$

where $n_1 = 4$ and $n_2 = -5/3$ are the exponents of the related magnetic energy spectrum, $\phi(\mathbf{k})$ are random phases, A_0 is the amplitude, and $k = |\mathbf{k}|$. We choose $k_0/k_1 = 60$ and run with $\nu = 5 \times 10^{-6}$ at 1152^3 mesh-points, which is slightly more dissipative than the runs reported in the Letter with $\nu = 2 \times 10^{-6}$ using 2304^3

meshpoints. In Fig. 6 we show the times $t/\tau_A = 10, 50, 200,$ and $900,$ where $\tau_A = (v_{A0}k_0)^{-1}$ is the initial Alfvén time.

At very early times ($t \approx \tau_A$), a k^4 kinetic energy spectrum develops, which is consistent with the causality constraint, but after several hundred Alfvén times the spectrum becomes gradually shallower and approaches a k^2 subinertial range. However, unlike the initial condition shown in Fig. 5, the magnetic field is continuously decaying and the integral scale is increasing, which is the reason why the k^2 subinertial range is less strongly developed in Fig. 6. Nevertheless, the magnetic spectrum shows again clear inverse transfer, although it is initially somewhat slower, as can be expected given the time it takes to build up the k^2 velocity spectrum.

Steeper initial spectra

If we start with a magnetic energy spectrum steeper than k^4 , the spectrum quickly changes into a k^4 . This is demonstrated in Fig. 7, where we start with an initial k^6 spectrum, followed by a $k^{-5/3}$ subrange. We show the times $t/\tau_A = 1, 5, 20, 80,$ and $400,$ and see that already at $t/\tau_A = 20$ the subinertial range has nearly a k^4 subrange.

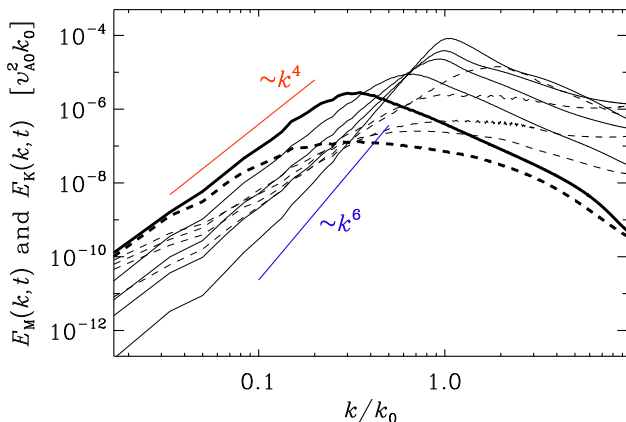


FIG. 7: Like Fig. 6, but with an initial k^6 spectrum for the magnetic energy using random phases.

Evolution

Integral scale

The decay of MHD turbulence is characterized by the kinetic and magnetic integral scales. The kinetic integral scale $\xi_K = k_K^{-1}$ is defined analogously to the magnetic

one $\xi_M = k_M^{-1}$ (given in the Letter), with

$$k_K^{-1}(t) = \int_0^\infty k^{-1} E_K(k, t) dk / \mathcal{E}_K(t). \quad (3)$$

Both scales grow in time nearly perfectly proportional to each other like $t^{1/2}$; see Fig. 8. The corresponding decay of kinetic and magnetic energies is proportional to t^{-1} and is addressed in Sec. of this Supplemental Material, where we plot $u_{\text{rms}} = (2\mathcal{E}_K)^{1/2}$ and $v_A = (2\mathcal{E}_M)^{1/2}$.

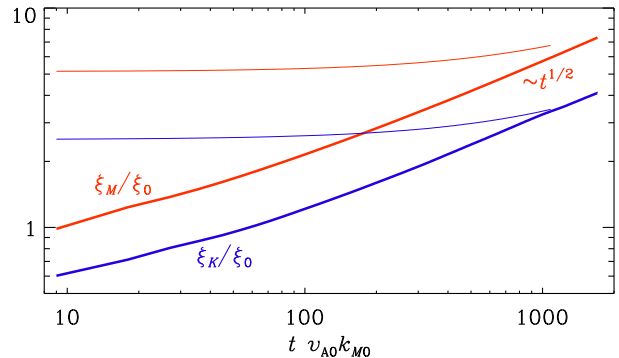


FIG. 8: Kinetic and magnetic integral scales, ξ_K and ξ_M , respectively, for Runs A (thick lines) and B (thin lines).

In Table 1 of Ref. [6], Campanelli has summarized the decay laws for various subinertial range scalings using both helical and non-helical MHD turbulence. The scaling exponent for the magnetic integral scale, $\xi_M^{-1}(t) = \int k^{-1} E_M(k, t) dk / \mathcal{E}_M(t)$, is around $1/2$ for most of the different cases. It emerges quite generically from scaling arguments first derived by [7]. Kalelkar & Pandit [8] find $\xi_M \sim t^{1/2}$ for an initial spectrum $E_M \sim k$, but the same scaling also emerges for other initial power laws, as has been demonstrated by numerous simulations [3–5]. The reason for this is that the decay properties depend mainly on nature of the turbulence (being either hydrodynamic, hydromagnetic without helicity, or with helicity).

Mach & Alfvén numbers

In Fig. 9, we plot the evolution of the Mach number u_{rms}/c_s , the Alfvén number u_{rms}/v_A , and the ratio v_A/c_s , where u_{rms} and v_A are the rms values of velocity and magnetic field (density is approximately constant), and $c_s = \text{const}$ is the isothermal sound speed.

Both u_{rms} and v_A decay in time proportional to $t^{-1/2}$, so the kinetic and magnetic energies decay like $\mathcal{E}_K(t) = u_{\text{rms}}^2/2 \propto t^{-1}$ and $\mathcal{E}_M(t) = v_A^2/2 \propto t^{-1}$. Earlier work [5] resulted in a decay law proportional to $t^{-0.9}$, but this departure from the t^{-1} law is likely a consequence of insufficient scale separation; k_0/k_1 is now 60 compared to 15 previously.

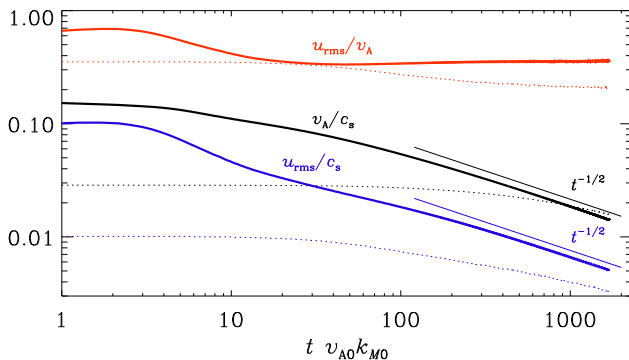


FIG. 9: Mach number u_{rms}/c_s (black), Alfvénic Mach number u_{rms}/v_A (red), and the ratio v_A/c_s (blue) for Runs A (thick, solid lines) and B (dotted lines).

Loitsyansky invariant

In hydrodynamic turbulence, using the constancy of the Loitsyansky invariant,

$$\mathcal{L} = \int \mathbf{r}^2 \langle \mathbf{u}(\mathbf{x}) \cdot \mathbf{u}(\mathbf{x} + \mathbf{r}) \rangle d\mathbf{r} \propto \ell^5 u_\ell^2, \quad (4)$$

with typical velocity u_ℓ on scale ℓ , Kolmogorov argued on dimensional grounds that the kinetic energy should decay like $\mathcal{E}_K \propto \mathcal{L}^{2/7} t^{-10/7}$. This decay law is close to the $t^{-5/4}$ scaling found in experiments [9] and simulations, including those using the PENCIL CODE [10].

This result has been generalized to MHD by Davidson [11], although no numerical confirmation of this has been mentioned in subsequent reviews [12]. On the other hand, if the decay is governed by viscosity, dimensional arguments suggest $\mathcal{E}_K \propto \nu t^{-1}$ and $\ell \propto (\nu t)^{1/2}$, both of which appear consistent with our simulations. If that is the case, we should expect \mathcal{L} to grow with time like $\mathcal{L} \propto \nu^{5/2} t^{1/2}$.

In Table II we give values of \mathcal{L} and $\langle \mathbf{u}^2 \rangle$ for a low resolution run (64^3 mesh points) and a down-sampled one of Run A of the Letter (2304^3 mesh points).

TABLE II: Values of \mathcal{L} and $\langle \mathbf{u}^2 \rangle$ for a low resolution run (64^3 mesh points) and a down-sampled one of Run A of the Letter (2304^3 mesh points).

resol.	t	\mathcal{L}	$\langle \mathbf{u}^2 \rangle$
64^3	40	$+2.1 \times 10^{-7}$	8.0×10^{-3}
	100	-5.4×10^{-7}	7.0×10^{-5}
	250	-8.4×10^{-7}	1.1×10^{-5}
2304^3	50	-4.4×10^{-9}	1.0×10^{-4}
	150	-1.1×10^{-8}	3.3×10^{-5}

Table II suggests that $|\mathcal{L}|$ has indeed a tendency to increase with time. This would support our argument

above in favor of viscously dominated decay behavior. On the other hand, as the resolution is increased by a factor of 36, \mathcal{L} decreases by about two orders of magnitude while u_{rms} stays about the same. This would be consistent with \mathcal{L} converging to zero and therefore not being able to constrain the decay.

Comparison with hydrodynamics

In the absence of magnetic fields, there is purely hydrodynamic decay without the mutual interaction between two energy reservoirs. This leads to a steeper decay law for kinetic energy and a slower growth of the integral scale, as can be easily be verified by applying an initial k^4 spectrum for the kinetic energy. This is shown in Fig. 10, where we compare the decay spectra for hydrodynamic turbulence with nonhelical and helical magnetohydrodynamic turbulence.

Scaling behavior

According to the Olesen scaling law [7], both kinetic and magnetic energies should decay like

$$E_K(k, t) \sim E_M(k, t) \sim k^\alpha \psi(k^{(3+\alpha)/2} t). \quad (5)$$

Integrating over k yields the decay law of the energies as

$$\mathcal{E}_K(t) = \int E_K(k, t) dk \sim \int k^\alpha \psi(k^{(3+\alpha)/2} t) dk. \quad (6)$$

Introducing $\kappa = kt^q$ with $q = 2/(3 + \alpha)$, we have

$$\mathcal{E}_K(t) \sim t^p \int \kappa^\alpha \psi(\kappa) d\kappa, \quad (7)$$

where $p = (1 + \alpha)q$. The integral scales like $k_K \sim t^q$ with $q = 2/(3 + \alpha)$. Several parameter combinations are given in Table III.

TABLE III: Parameter combinations of $q = 2/(3 + \alpha)$, $p = 2(1 - q)$ and $\alpha = 2/q - 3$. Note that $10/7 \approx 1.43$ and $2/7 = 0.286$.

$\alpha (= \beta)$	p	q	physics
4	10/7	2/7	$\mathcal{L} = \text{const}$
3	8/6	2/6	
2	6/5	2/5	
1	4/4	2/4	$\langle \mathbf{A}_{2D}^2 \rangle = \text{const} ?$
0	2/3	2/3	$\langle \mathbf{A} \cdot \mathbf{B} \rangle = \text{const}$

The numbers in Table III suggest that different subinertial range scalings $\propto k^\alpha$ correspond to different exponents p and q . Instead, we now argue that the subinertial range scaling is not characterized just by α , but

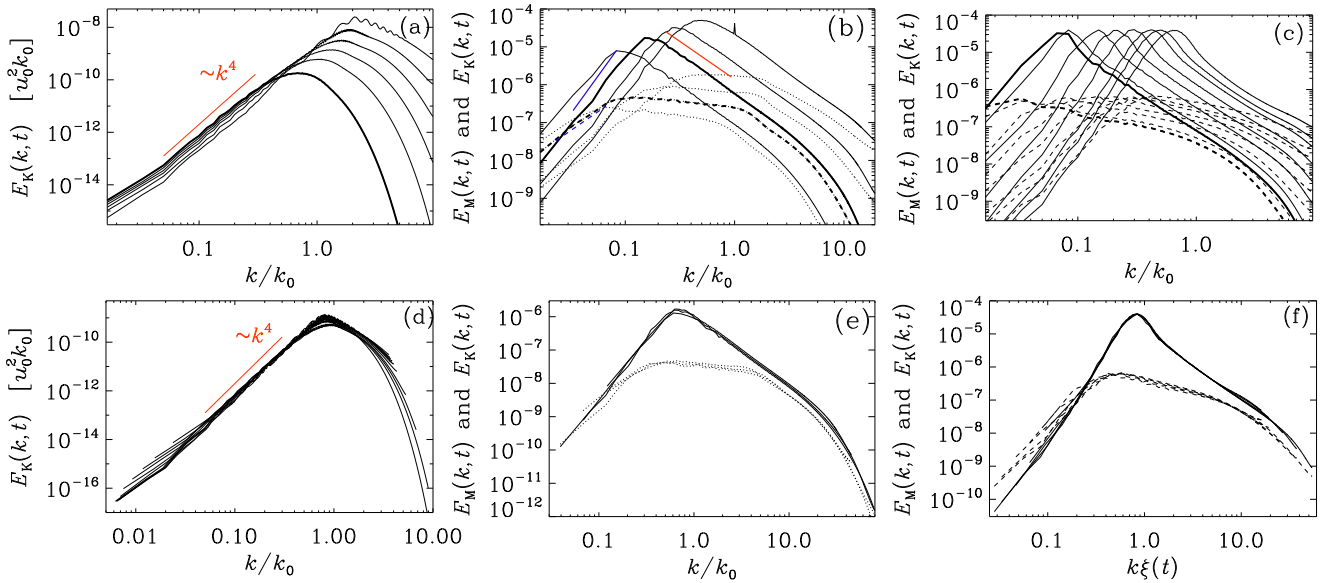


FIG. 10: Kinetic energy spectra in a hydrodynamic simulation (a), compared with magnetic (solid) and kinetic (dashed) energy spectra in a hydromagnetic simulation without helicity (b), and with (c). Panels (d)–(f) show the corresponding collapsed spectra obtained by using $\beta = 3$ (d), $\beta = 1$ (e), and $\beta = 0$ (f).

mainly by the slope of $\psi(k)$ for small values of k . To demonstrate this, let us begin by noting that, in practice, it is more accurate to relate the change in the amplitude to the change in the correlation length instead of the time, because it always takes a while to establish asymptotic scaling behavior. Therefore, instead of using Equation (5), we prefer the following alternative formulation by extracting just a time-dependent factor from the spectrum and write [13]

$$E_M(k, t) \sim \xi^\beta \phi(k\xi), \quad (8)$$

with $\xi(t) \sim t^q$ standing either for ξ_M (in the magnetic case) or for ξ_K (in the hydrodynamic case). The exponent q can be determined by dimensional arguments, e.g. by assuming $\mathcal{L} = \text{const} = U^2 L^5$, which implies

$$\mathcal{L} \sim u^2 l^5 \sim l^7 \tau^{-2} \rightarrow q = 2/7, p = 10/7 (\beta = 4). \quad (9)$$

Alternatively, in the presence of helical magnetic fields, $\langle \mathbf{A} \cdot \mathbf{B} \rangle$ is conserved. Again, from dimensional arguments we find

$$\langle \mathbf{A} \cdot \mathbf{B} \rangle \sim u^2 l \sim l^3 \tau^{-2} \rightarrow q = 2/3, p = 2/3 (\beta = 0). \quad (10)$$

Finally, in nonhelical hydromagnetic turbulence we have $q = 1/2$, which suggests that a quantity with the dimensions $u^2 l^2$ should be constant. Since $\langle \mathbf{A}^2 \rangle / \mu_0 \rho_0$ has such dimensions $u^2 l^2$, we must carefully reassess our previous findings suggesting that the flow is fully three-dimensional. Nevertheless, tentatively one can state

$$\langle \mathbf{A}_{2D}^2 \rangle \sim u^2 l^2 \sim l^4 \tau^{-2} \rightarrow q = 1/2, p = 1 (\beta = 1), \quad (11)$$

where \mathbf{A}_{2D} is the gauge that aligns \mathbf{A} with the intermediate rate-of-strain vector; see Sec. . Equations (9)–(11) a decay law $E_M \sim t^{-p}$ with $p = (1 + \beta)q$, where β is a parameter that is usually *not* associated with the subinertial range scaling exponent α . Formally, however, we find that $\alpha = \beta$, so the parameter combinations in Table III still apply with $\alpha = \beta$, but this new formulation does not imply anything about the subinertial range scaling.

Inverse transfer

The growth of spectral energy at small wavenumbers is cautiously referred to as *inverse transfer*. By contrast, in an *inverse cascade* there is a k -independent flux of some quantity (e.g., of magnetic helicity in three-dimensional hydromagnetic turbulence) toward progressively smaller k . An inverse cascade is known to exist in three dimensional hydromagnetic turbulence if there is helicity. Also two-dimensional hydrodynamic turbulence is known to exhibit inverse cascade behavior.

While any of these mechanisms could in principle play a role in explaining the behavior seen in the Letter [1], there may also be completely different mechanisms that could potentially explain the growth of spectral magnetic energy at large length scales. In order to narrow down possible reasons for the inverse transfer found in our simulations, we begin by discussing the concepts of eddy noise and the unwinding of magnetic fields. We also determine the magnetic helicity as well as various other helicities and examine whether the flow could be locally two-dimensional, which might provide yet another cause

of inverse transfer, in which case one could appeal to the inverse cascade of $\langle \mathbf{A}_{2D}^2 \rangle$, where \mathbf{A}_{2D} is the magnetic vector potential perpendicular in a gauge in which it is locally aligned with the intermediate eigenvector of the rate-of-strain tensor.

Eddy noise

Eddy noise has been mentioned as a mechanism that brings energy from the unresolved scales into resolved scales [14, 15]. The physics of this mechanism is obscured by the fact that it referred originally to numerical artifacts. In particular, it is not obvious that it really leads to a spectral increase of power rather than just a preferential decay at small scales. Of course, at a descriptive level, the concept of eddy noise may be similar to what we find, although there was never a clear demonstration of the resulting spectral evolution.

Unwinding magnetic fields

One could imagine that the unwinding of a magnetic field leads to the conditions seen in the Letter. Again, this is only a descriptive concept, but one could think of addressing this question through a numerical experiment. Winding up an externally imposed magnetic field leads to magnetic flux expulsion, as first shown by Weiss [16]. We now ask about the dynamical behavior of such a magnetic field after the driving force is turned off.

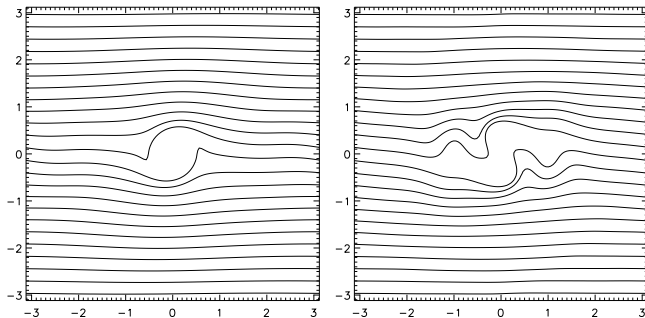


FIG. 11: Field lines in a two-dimensional simulation in the presence of a forced hydromagnetic eddy at an intermediate time (left) and a later time (right) when the eddy has been altered by the Lorentz force in a time-dependent manner.

There are several complications with this seemingly simple idea. First, the original problem of Weiss was not dynamic, but kinematic. Allowing the flow to be a self-consistent solution of the momentum equation leads to more complicated behavior, as demonstrated in Fig. 11, where the driving force is given by $\mathbf{f} = \nabla \times \psi \hat{\mathbf{z}}$ with $\psi = \cos k_1 x \cos k_1 y \exp(-r^2/2R^2)$, and $r^2 = x^2 + y^2$. Second,

turning off the driving leads to propagating Alfvén waves and long-term oscillations at large scales, which is very different from what is seen in the Letter. However, this behavior can easily be removed by also turning off the imposed magnetic field. Finally, the eddy shown in Fig. 11 is too big ($R = 0.1$) and there would be no extended subinertial range. Thus, we now repeat this experiment with a much smaller eddy of radius $R = 0.002$. The resulting spectral evolution is shown in Fig. 12.

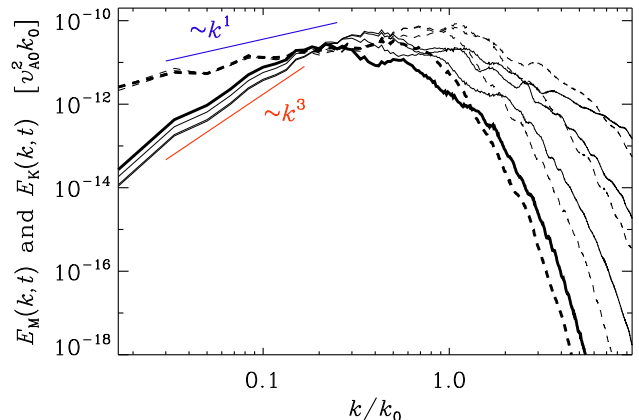


FIG. 12: Kinetic and magnetic energy spectra. The two red lines are proportional to k^1 and k^3 , respectively.

In this experiment, the initial magnetic field is a global one and it therefore unconstrained by causality. It turns out that the magnetic energy now has a k^3 subrange at large scales. Interestingly, as the magnetic field decays, there is a slight decay also at large length scales, so there is no inverse transfer in such a setup.

Helicities for Runs A and B

In Table IV we list various helicities for Runs A and B. The normalized kinetic helicity $\langle \boldsymbol{\omega} \cdot \mathbf{u} \rangle / \omega_{\text{rms}} u_{\text{rms}}$ and the normalized cross helicity $2\langle \mathbf{u} \cdot \mathbf{b} \rangle / (u_{\text{rms}}^2 + b_{\text{rms}}^2)$ are less than 0.4%, the normalized current helicity $\langle \mathbf{j} \cdot \mathbf{b} \rangle / j_{\text{rms}} b_{\text{rms}}$ is less than 2%, and the normalized magnetic helicity $k_1 \langle \mathbf{a} \cdot \mathbf{b} \rangle / b_{\text{rms}}^2$ is less than 1%. In this Letter, it was shown that the level of magnetic helicity was small enough so as not to constrain (i.e., enhance) the growth of the integral scale. Also the other helicities appear to be small enough for being important in explaining the inverse transfer.

Projections onto strain tensor

To examine whether there is a tendency for the turbulence to become locally two-dimensional, we compute

TABLE IV: Various helicities for Run A of the Letter.

quantity	expression	value
kinetic hel.	$\langle \boldsymbol{\omega} \cdot \mathbf{u} \rangle / \omega_{\text{rms}} u_{\text{rms}}$	0.00364
current hel.	$\langle \mathbf{j} \cdot \mathbf{b} \rangle / j_{\text{rms}} b_{\text{rms}}$	0.01693
cross hel.	$2\langle \mathbf{u} \cdot \mathbf{b} \rangle / (u_{\text{rms}}^2 + b_{\text{rms}}^2)$	-0.00318
magnetic hel.	$k_1 \langle \mathbf{a} \cdot \mathbf{b} \rangle / b_{\text{rms}}^2$	0.00976

the rate-of-strain tensor,

$$s_{ij} = \frac{1}{2} (u_{i,j} + u_{j,i}). \quad (12)$$

Since s_{ij} is symmetric, it has three real eigenvalues, λ_i for $i = 1, 2$, and 3. They are traditionally ordered such that

$$\lambda_1 < \lambda_2 < \lambda_3. \quad (13)$$

The corresponding eigenvectors are called \hat{e}_i .

If the flow was incompressible, their sum would vanish, which is here also approximately the case. The largest eigenvalue λ_3 corresponds to stretching in the direction \hat{e}_3 , and the most negative one, λ_1 , corresponds to compression in the direction \hat{e}_1 .

It has been known for some time [17, 18] that in isotropic turbulence the vorticity vector tends to be aligned with the direction \hat{e}_2 and is therefore normal to the plane where the flow would be two-dimensional. If the turbulence was perfectly two-dimensional, the intermediate eigenvalue of the rate-of-strain tensor would vanish. This is however not the case; see Fig. 13, where we plot probability density functions (PDFs) of the three eigenvalues.

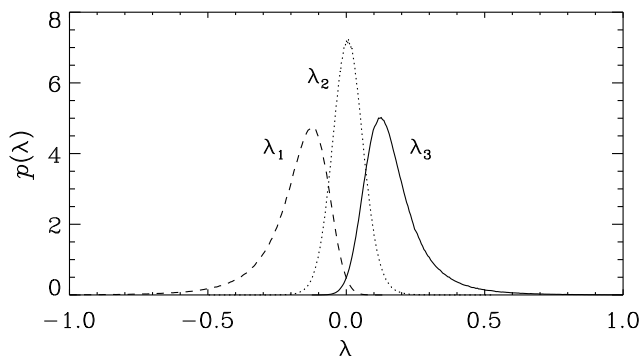


FIG. 13: PDF of the eigenvalues of the rate-of-strain tensor. Note that the intermediate ones are not vanishing, as expected for two-dimensional turbulence.

In the present simulations, we see all the usual characteristics of three-dimensional MHD turbulence where the vorticity vector $\boldsymbol{\omega}$ is aligned with the eigenvector \hat{e}_2 .

Also the magnetic field \mathbf{B} is aligned with \hat{e}_2 ; see Fig. 14. Here, the PDFs $p(\cos \phi)$ are normalized such that

$$\int_0^1 p(\cos \phi) d \cos \phi = 1. \quad (14)$$

Furthermore, while $\boldsymbol{\omega}$ is perpendicular to \hat{e}_1 and \hat{e}_3 , the angle between \mathbf{B} and both \hat{e}_1 and \hat{e}_3 is about 45° (see lower panel of Fig. 14), which was first found in MHD shear flows; see Ref. [19], who interpreted their finding as alignment with the direction of the overall shear. In this connection we recall that a shear flow can be decomposed into a rotational and a straining motion [20]. The rotational motion is not captured by the strain tensor. The directions of compression and stretching are then at 45° angles with respect to the direction of the shear [21]. Similar results have recently also been obtained in Ref. [22].

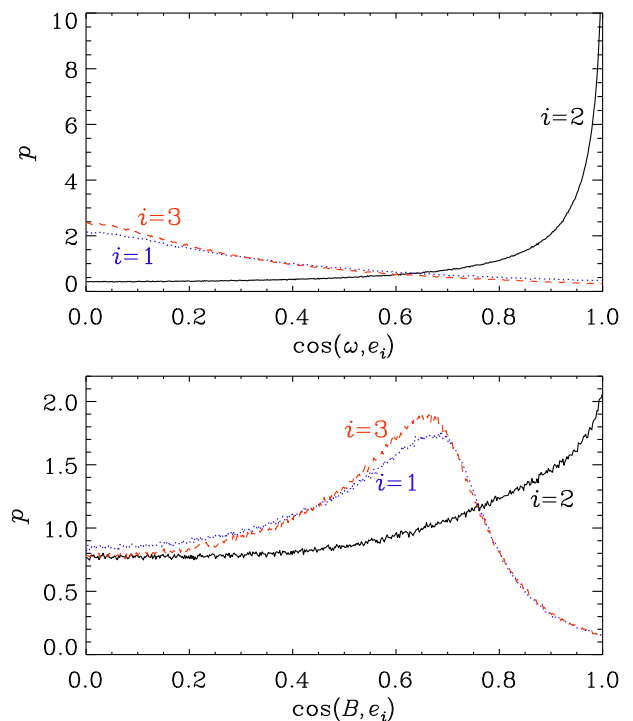


FIG. 14: Alignment of $\boldsymbol{\omega}$ and \mathbf{B} with the eigenvectors of the rate-of-strain tensor.

Next, we compute the projections of various vectors $\boldsymbol{\sigma}$ onto s_{ij} :

$$s_\sigma = \langle \sigma_i s_{ij} \sigma_j \rangle / \langle \sigma^2 \rangle, \quad (15)$$

where $\boldsymbol{\sigma}$ is either \mathbf{u} , $\boldsymbol{\omega}$, \mathbf{B} , or \mathbf{J} . For $\boldsymbol{\omega}$ and \mathbf{B} , these values quantify the production of $\boldsymbol{\omega}$ and \mathbf{B} , respectively, but for the other quantities no such interpretation exists. In Table V we give the mean and rms values of the s_σ . Here we also compare with the projection of \mathbf{A} onto the

TABLE V: Mean and rms values of the normalized projections \mathbf{s}_σ with $\sigma = \mathbf{u}, \boldsymbol{\omega}, \mathbf{B}$, and \mathbf{J} onto s_{ij} and a comparison with the value of \mathbf{s}_A defined in the text.

σ	\mathbf{u}	$\boldsymbol{\omega}$	\mathbf{B}	\mathbf{J}	\mathbf{A}
mean	0.009	0.019	-0.001	0.005	0.007
rms	0.145	0.204	0.069	0.064	0.106

direction $\hat{\mathbf{e}}_2$, i.e., $\mathbf{A} \rightarrow \hat{\mathbf{e}}_2(\mathbf{A} \cdot \hat{\mathbf{e}}_2)$, and therefore $\mathbf{s}_A = \langle \lambda_2(\mathbf{A} \cdot \hat{\mathbf{e}}_2)^2 \rangle / \langle (\mathbf{A} \cdot \hat{\mathbf{e}}_2)^2 \rangle$.

Note that \mathbf{s}_A is not particularly small, as one would have expected for a locally nearly two-dimensional flow and is comparable to all the other terms. The average of $\langle B_i s_{ij} B_j \rangle / \langle \mathbf{B}^2 \rangle$ is actually the smallest one among them all.

Conservation of squared potential?

In the Letter, we have argued that the inverse transfer can be a consequence of the different subinertial range scalings for kinetic and magnetic energy spectra. However, as a very different possibility we also have to consider an inverse cascade due to the approximate invariance of $\langle \mathbf{A}^2 \rangle$ in two dimensions. This would seem surprising given the similar widths of the PDFs of the intermediate eigenvalue λ_2 and those of λ_1 and λ_3 , which suggests that the flow cannot be regarded as locally two-dimensional.

The quantity $\langle \mathbf{A}^2 \rangle$ is obviously gauge-dependent. However, the relevant gauge is one that aligns \mathbf{A} locally with $\hat{\mathbf{e}}_2$. Thus, we use the new vector potential

$$\mathbf{A}_{2D} = \mathbf{A} + \nabla \Lambda, \quad (16)$$

such that

$$0 = \hat{\mathbf{e}}_2 \times \mathbf{A} + \hat{\mathbf{e}}_2 \times \nabla \Lambda, \quad (17)$$

Taking the curl yields

$$0 = \hat{\mathbf{e}}_2 \cdot \nabla \times (\hat{\mathbf{e}}_2 \times \mathbf{A}) + \hat{\mathbf{e}}_2 \cdot \nabla \times (\hat{\mathbf{e}}_2 \times \nabla \Lambda), \quad (18)$$

which can be solved in Fourier space (indicated by hats) to give

$$\nabla \Lambda = - \int \frac{\mathbf{k} \cdot \hat{\mathbf{A}} - (\hat{\mathbf{e}}_2 \cdot \mathbf{k})(\hat{\mathbf{e}}_2 \cdot \hat{\mathbf{A}})}{\mathbf{k}^2 - (\hat{\mathbf{e}}_2 \cdot \mathbf{k})^2} \mathbf{k} e^{i\mathbf{k} \cdot \mathbf{x}} d^3 k, \quad (19)$$

In Table VI we summarize the values of $\langle \mathbf{A}^2 \rangle$ (in the gauge used in the code, i.e., the Weyl gauge) and $\langle \mathbf{A}_{2D}^2 \rangle$, and compare their temporal changes with that of $\langle \mathbf{B}^2 \rangle$ for a low resolution run and the down-sampled Run A of the Letter. Note first of all that $\langle \mathbf{A}_{2D}^2 \rangle$ is always smaller than $\langle \mathbf{A}^2 \rangle$. This is expected, because \mathbf{A} contains redundant contributions. Second, $\langle \mathbf{A}_{2D}^2 \rangle$ decays more slowly

TABLE VI: Values of $\langle \mathbf{A}^2 \rangle$, $\langle \mathbf{A}_{2D}^2 \rangle$, and $\langle \mathbf{B}^2 \rangle$ for a low resolution run (144^3 mesh points) and the down-sampled Run A of the Letter (2304^3 mesh points).

resol.	t	$\langle \mathbf{A}^2 \rangle$	$\langle \mathbf{A}_{2D}^2 \rangle$	$\langle \mathbf{B}^2 \rangle$
144^3	10	1.8×10^{-5}	9.7×10^{-6}	1.8×10^{-4}
	50	1.2×10^{-5}	6.0×10^{-6}	8.1×10^{-5}
	100	9.4×10^{-6}	5.1×10^{-6}	4.4×10^{-5}
	200	6.6×10^{-6}	5.0×10^{-6}	2.0×10^{-5}
2304^3	50	5.3×10^{-5}	2.0×10^{-5}	8.2×10^{-4}
	100	4.4×10^{-5}	9.9×10^{-6}	4.0×10^{-4}
	150	4.0×10^{-5}	8.7×10^{-6}	2.6×10^{-4}

than $\langle \mathbf{B}^2 \rangle$, demonstrating that $\langle \mathbf{A}_{2D}^2 \rangle$ is approximately conserved. Furthermore, the ratio $(\langle \mathbf{A}_{2D}^2 \rangle / \langle \mathbf{B}^2 \rangle)^{1/2}$ is a length scale of around 0.2 for Run A, which is well above the scale Taylor micro scale shown in Fig. 4 of the Letter. Thus, the typical values of $\langle \mathbf{A}_{2D}^2 \rangle$ may well be significant for explaining the $\xi_M \sim t^{1/2}$ scaling and its approximate conservation could be responsible for the inverse cascade [23].

Reynolds and Lundquist numbers

Since u_{rms} , v_A , and k_M are all proportional to $t^{-1/2}$ the decay is self-similar in such a way that the Reynolds and Lundquist numbers, $\text{Re} = u_{\text{rms}}/\nu k_M$ and $\text{Lu} = v_A/\eta k_M$, remain constant. This is clearly demonstrated in Fig. 15, where we plot Re (dotted) and Lu (solid) both for Runs A and B with $\text{Pr}_M = 1$ and 10, respectively.

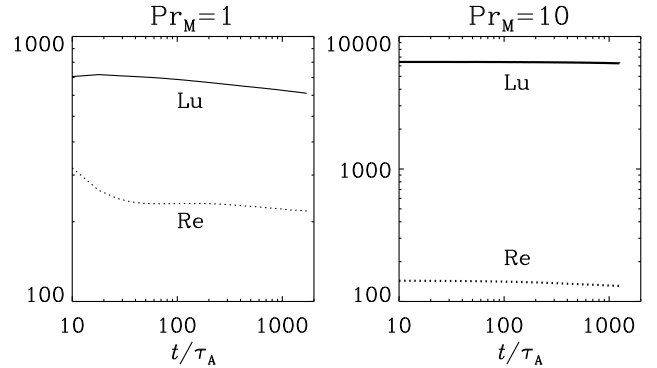


FIG. 15: Instantaneous magnetic and kinetic Reynolds numbers for Runs A and B with $\text{Pr}_M = 1$ and 10, respectively.

During the decay, the approximate values of Re and Lu are 230 and 700 for Run A and 130 and 6300 for Run B. As discussed in the Letter, for Run B the value of Lu is so huge that, even though we also have a large number of mesh points, one must be concerned about the numerical

accuracy of the simulation. One should note, however, that, because $\text{Pr}_M = 10$ is larger than unity, most of the energy is dissipated viscously. Therefore, although Lu is huge, less magnetic energy needs to be dissipated than for $\text{Pr}_M = 1$. This was demonstrated first in Ref. [24] for the opposite case with $\text{Pr}_M \ll 1$ (where Joule dissipation dominates) and later, in Refs. [25, 26], for $\text{Pr}_M \gg 1$, which is the case relevant here.

Energy transfers

In the Letter we considered the spectral transfer function $T_{kpq} = \langle \mathbf{J}^k \cdot (\mathbf{u}^p \times \mathbf{B}^q) \rangle$, which governs the gain of magnetic energy and correspondingly the loss of kinetic energy. There is also a kinetic energy transfer function S_{kpq} , which describes the transfer between different scales. It vanishes for $k = p$ and is given by $S_{kpq} = \rho_0 \langle \mathbf{u}^k \cdot (\mathbf{u}^p \times \boldsymbol{\omega}^q) \rangle$, where $\rho_0 = \langle \rho \rangle$ is the average density; compressibility effects have been ignored here. The transfer function S_{kpq} enters only in the kinetic energy equation. Thus, the magnetic and kinetic energy equations are given by

$$\frac{d}{dt} \langle \frac{1}{2} \mathbf{B}_k^2 \rangle = T_{kpq} - \eta k^2 \langle \mathbf{B}_k^2 \rangle, \quad (20)$$

$$\frac{d}{dt} \langle \frac{1}{2} \rho_0 \mathbf{u}_p^2 \rangle = -T_{kpq} - S_{kpq} - \nu p^2 \langle \rho_0 \mathbf{u}_p^2 \rangle. \quad (21)$$

Swapping indices k and p in Equation (21) yields

$$\frac{d}{dt} \langle \frac{1}{2} \rho_0 \mathbf{u}_k^2 \rangle = -T_{pkq} - S_{pkq} - \nu k^2 \langle \rho_0 \mathbf{u}_k^2 \rangle. \quad (22)$$

To get the total energy at wavenumber k , we now add Equations (20) and (22), i.e.,

$$\frac{1}{2} \frac{d}{dt} \langle \mathbf{B}_k^2 + \rho_0 \mathbf{u}_k^2 \rangle = T_{kpq} - T_{pkq} - S_{pkq} - \eta k^2 \langle \mathbf{B}_k^2 \rangle - \nu k^2 \langle \rho_0 \mathbf{u}_k^2 \rangle. \quad (23)$$

The total energy has contributions from all p and q and it is of interest to separate between those that are larger and smaller than k , so we write

$$\frac{1}{2} \frac{d}{dt} \langle \mathbf{B}_k^2 + \rho_0 \mathbf{u}_k^2 \rangle = \Pi_{p \geq k}^{q \geq k} + \Pi_{p \geq k}^{q < k} + \Pi_{p < k}^{q \geq k} + \Pi_{p < k}^{q < k} - \eta k^2 \langle \mathbf{B}_k^2 \rangle - \nu k^2 \langle \rho_0 \mathbf{u}_k^2 \rangle. \quad (24)$$

where

$$\Pi_{p \geq k}^{q < k} = \sum_{p \geq k} \sum_{q < k} (T_{kpq} - T_{pkq} - S_{pkq}). \quad (25)$$

The results in Fig. 16 show that $\Pi_{p < k}^{q < k}$ is positive for $k/k_0 > 0.25$, demonstrating that there is a gain of total energy at wavenumbers $k/k_0 > 0.25$ from interactions

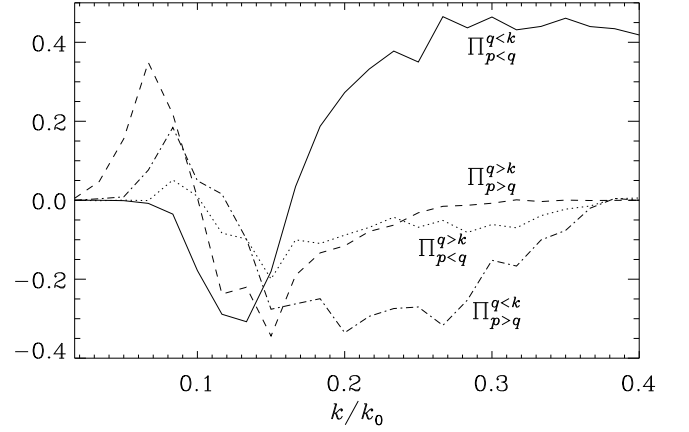


FIG. 16: Energy transfer functions defined in Equation (25).

with smaller wavenumbers. This shows that there is forward transfer at those wavenumbers. Furthermore, for $k/k_0 > 0.25$, the spectral transfer is approximately independent of k , as expected for a proper forward cascade. There is also a short range $0.15 < k/k_0 < 0.3$, where $\Pi_{p < k}^{q < k}$ is negative. This suggests the existence of inverse transfer resulting from mixed interactions of $p > k$ and $q < k$. In our simulations, $|T_{kpq}|$ dominates over $|S_{kpq}|$, so the dominant contribution to wavenumbers q comes from the magnetic field.

Concluding remarks

The decay of magnetically dominated MHD turbulence is a rich field, sharing several similarities with the case in which the magnetic field is dynamo-generated, for example the alignment properties with the eigenvectors of the rate-of-strain tensor. In the Letter, we have focussed on the inverse transfer properties that were previously only known for helical MHD turbulence. This is a new and exciting result that has now been confirmed by two additional independent groups [27, 28]. The results presented in the Supplemental Material support the robustness of this result and suggest that the inverse transfer is not explained by other previously studied mechanisms.

-
- [1] A. Brandenburg, T. Kahniashvili, and A. G. Tevzadze, Phys. Rev. Lett., submitted, arXiv:1404.2238 (2014).
 - [2] A. Brandenburg, K. Enqvist, and P. Olesen, Phys. Rev. D **54**, 1291 (1996).
 - [3] T. Kahniashvili, A. Brandenburg, A. G. Tevzadze and B. Ratra, Phys. Rev. D **81**, 123002 (2010).
 - [4] A. G. Tevzadze, L. Kisslinger, A. Brandenburg and T. Kahniashvili, Astrophys. J. **759**, 54 (2012).

- [5] T. Kahniashvili, A. G. Tevzadze, A. Brandenburg and A. Neronov, *Phys. Rev. D* **87**, 083007 (2013)
- [6] L. Campanelli, *Eur. Phys. J. C* **74**, 2690 (2014).
- [7] P. Olesen, *Phys. Lett. B* **398**, 321 (1997).
- [8] C. Kalelkar and R. Pandit, *Phys. Rev. E* **69**, 046304 (2004).
- [9] H. S. Kang, S. Chester, and C. Meneveau, *J. Fluid Mech.* **480**, 129 (2003).
- [10] N. E. L. Haugen and A. Brandenburg, *Phys. Rev. E* **70**, 026405 (2004).
- [11] P. A. Davidson, *J. Turb.* **1**, 006 (2000).
- [12] P. A. Davidson, *J. Fluid Mech.* **663**, 268 (2010).
- [13] M. Christensson, M. Hindmarsh, and A. Brandenburg, *Phys. Rev. E* **64**, 056405 (2001).
- [14] J. Baerenzung, H. Politano, Y. Ponty, and A. Pouquet, *Phys. Rev. E* **77**, 046303 (2008).
- [15] A. Sen, P. D. Mininni, D. Rosenberg, and A. Pouquet, *Phys. Rev. E* **86**, 036319 (2012).
- [16] N. O. Weiss, *Proc. Roy. Soc. Lond. A* **293**, 310 (1966).
- [17] R. M. Kerr, *J. Fluid Mech.* **153**, 31 (1985).
- [18] W. T. Ashurst, A. R. Kerstein, R. M. Kerr, and C. H. Gibson, *Phys. Fluids* **30**, 2343 (1987).
- [19] A. Brandenburg, Å. Nordlund, R. F. Stein, and I. Toroksson, *Astrophys. J.* **446**, 741 (1995).
- [20] A. Brandenburg, *Chaos, Solitons & Fractals* **5**, 2025 (1995).
- [21] A. Brandenburg, R. L. Jennings, Å. Nordlund, M. Rieutord, R. F. Stein, and I. Tuominen, *J. Fluid Mech.* **306**, 325 (1996).
- [22] S. Sur, L. Pan, and E. Scannapieco, *Astrophys. J.* **790**, L9 (2014).
- [23] A. Pouquet, *J. Fluid Mech.* **88**, 1 (1978).
- [24] A. Brandenburg, *Astrophys. J.* **697**, 1206 (2009).
- [25] A. Brandenburg, *Astron. Nachr.* **332**, 51 (2011).
- [26] A. Brandenburg, *Astrophys. J.* **791**, 12 (2014).
- [27] A. Berera and M. Linkmann, *Phys. Rev. E* **90**, 041003 (2014).
- [28] J. Zrake, *Astrophys. J.* **794**, L26 (2014).